## **RESEARCH ARTICLE**

WILEY

## An investigation into remote sensing techniques and field observations to model hydraulic roughness from riparian vegetation

Smriti Chaulagain | Mark C. Stone | Daniel Dombroski | Tyler Gillihan | Li Chen<sup>3</sup> | Su Zhang<sup>1,4</sup>

#### Correspondence

Mark C. Stone, Department of Civil, Construction, and Environmental Engineering, University of New Mexico, Albuquerque, NM,

Email: stone@unm.edu

#### **Funding information**

National Science Foundation, Grant/Award Numbers: 1641289, 1254569

#### Abstract

Riparian vegetation provides many noteworthy functions in river and floodplain systems, including its influence on hydrodynamic processes. Traditional methods for predicting hydrodynamic characteristics in the presence of vegetation involve the application of static Manning's roughness, which does not directly account for vegetation characteristics and neglects changes in roughness due to local water depth and velocity. The objectives of this study were to (1) implement numerical routines for simulating vegetation-induced hydraulic roughness in a two-dimensional (2D) hydrodynamic model; (2) evaluate the performance of two vegetation roughness approaches; and (3) compare vegetation parameters and hydrodynamic model results based on field-based and remote sensing acquisition methods. Two roughness algorithms were coupled to an existing 2D hydraulic solver, which requires vegetation parameters to calculate spatially distributed roughness coefficients. Vegetation parameters were determined by field survey and using airborne light detection and ranging (LiDAR) data for San Joaquin River, California, USA. Water surface elevations modeled using vegetation-based roughness approaches produced an acceptable overall performance, but the results were sensitive to the vegetation parameterization method (field based vs. LiDAR). Spatial variations in roughness and hydraulic conditions (water depth and velocity) were observed based on vegetation species and discharges for vegetation-based approaches. The proposed approach accounts for the complexities of the physical environment instead of relying on traditional roughness as model inputs. Thus, the method proposed here is beneficial for describing the hydraulic conditions for the area having spatial variation of vegetation (e.g., species and density). However, additional research is needed to quantify model performance with respect to spatially distributed water depth and velocity and parameterization of vegetation characteristics.

## **KEYWORDS**

hydraulic roughness, LiDAR, riparian vegetation, San Joaquin River, SRH-2D, two-dimensional hydraulic modeling, vegetation parameters

.351476, 2022, 10. Downloaded from https://onlinelibrary.wiley.com/doi/10.1002/rra.4053 by University Of New Mexico, Wiley Online Library on [12/1/20202]. See the Terms and Conditions (https://onlinelibrary.wiley.com/rems-and-conditions) on Wiley Online Library for rules of use; OA articles are governed by the applicable Creative Commons In the Common of the Commo

<sup>&</sup>lt;sup>1</sup>Department of Civil, Construction, and Environmental Engineering, University of New Mexico, Albuquerque, New Mexico, USA

<sup>&</sup>lt;sup>2</sup>Sedimentation and River Hydraulics, United States Bureau of Reclamation, Denver, Colorado, USA

<sup>&</sup>lt;sup>3</sup>School of Hydrology and Water Resources, Naniing University of Information Science and Technology, Nanjing, China

<sup>&</sup>lt;sup>4</sup>Earth Data Analysis Center, University of New Mexico, Albuquerque, New Mexico, USA

#### 1 | INTRODUCTION

Riparian vegetation plays many important roles in the hydraulic, geomorphic, and ecological processes of river systems (Butterfield et al., 2020; Dufour & Rodríguez-González, 2019; Gurnell, 2014; Naiman, Decamps, & Pollock, 1993; Solari et al., 2016). The ecological services provided by riparian vegetation are beneficial to both the river system and the residents in proximity to the river system (Groffman et al., 2003). Examples of these services include control of sediment transport mechanism (Västilä & Järvelä, 2018), water quality improvement (Dosskey et al., 2010), nutrient cycling (Hamilton, 2012), habitat provisioning (Richardson et al., 2007), and flood damage mitigation (Brauman, Daily, Duarte, & Mooney, 2007; Lawrence, Pindilli, & Hogan, 2019; Sholtes & Doyle, 2011). The ecological services associated with riparian zones have been severely degraded in many river systems as the result of river engineering, floodplain development, and watershed development (Croke, Thompson, & Fryirs, 2017; Picco, Comiti, Mao, Tonon, & Lenzi, 2017; Poff et al., 1997; Shafroth, Stromberg, & Patten, 2002; Sweeney et al., 2004).

While riparian vegetation is an integral part of maintaining a river's physical structure and ecological processes, it also increases local flood risk by reducing effective flow areas (Uotani, Kanda, & Michioku, 2014) and by increasing hydraulic roughness/resistance (Green, 2005; Rhee, Woo, Kwon, & Ahn, 2008; Wilson, Stoesser, & Bates, 2005). To reduce local flood risk, it is preferred to minimize flow resistance in sites that are sensitive to flooding (Darby, 1999; Masterman & Thorne, 1992). At the reach scale, hydraulic roughness affects the velocity, shear stress distribution, and momentum exchanges (Proust et al., 2013; Stone & Hotchkiss, 2007; Vermaas, Uijttewaal, & Hoitink, 2011). However, vegetation-induced roughness enhances flood wave attenuation (Anderson, Rutherfurd, & Western, 2006; Byrne, 2017) at the watershed scale.

The Chezy's coefficient, Darcy friction factor, and Manning's roughness coefficient (n) are most commonly used to represent the hydraulic roughness due to surface characteristics (Chanson, 2004). However, Manning's *n* is most popular among hydrologists. Manning's n is typically assumed to be a constant value (static) for a given channel location without considering hydraulic conditions (e.g., water depth and velocity) and the seasonality of vegetation. Traditionally, it is defined manually as a function of land cover type (Forzieri, Moser, Vivoni, Castelli, & Canovaro, 2010) based on predefined roughness values (Chow, 1959), reference photographs (e.g., Hicks & Mason, 1991), empirical formulas as a function of bed material (e.g., Wong & Parker, 2006), or through experts' visual inspection (Stone et al., 2013). The appropriateness of assuming that the value of n is a constant depends on the situation. It is appropriate to use a static *n* in some physical conditions such as non-vegetated channels and floodplains because the influence on hydraulic conditions is minimal (Kim, 2010; Wohl, 1998). However, the assumption of a static n value in the presence of vegetation can produce an inaccurate estimation of water depth and velocity (e.g., Abu-Aly et al., 2014; Curran & Hession, 2013; Curran & Wohl, 2003; Fathi-Maghadam & Kouwen, 1997; Hession & Curran, 2013; Marcus, Roberts, Harvey, &

Tackman, 1992) because the vegetative drag is the dominant force affecting the roughness. The roughness due to vegetation depends on hydraulic conditions as well as the vegetation characteristics (Baptist et al., 2007; Järvelä, 2004). To model complex physical environments, it is essential to include the dynamic effects of vegetation and accurately represent hydraulic roughness.

The physical mechanism for generating hydraulic roughness by induced drag forces ultimately dictates the sensitivity of *n* to hydraulic conditions. Vegetation-induced flow resistance is primarily generated by form drag, which is highly dependent on velocity (Kouwen & Fathi Moghadam, 2000). Flow depth also strongly influences hydraulic roughness regarding vegetation submergence (Carollo, Ferro, & Termini, 2005; Järvelä, 2004; Wu, Shen, & Chou, 1999). In the case of submerged vegetation, the relative submergence (water depth/plant height) influences the boundary layer and vertical velocity distribution (Nepf & Ghisalberti, 2008). If the vegetation is emergent, the projected area of vegetation (momentum absorbing area) interacting with the moving water is a function of water depth (Lightbody & Nepf, 2006; Nepf, 1999).

A number of approaches have been proposed for estimating roughness coefficients in the presence of vegetation (e.g., Baptist et al., 2007; Fathi-Maghadam & Kouwen, 1997; Järvelä, 2004; Kouwen & Li, 1980; Petryk & Bosmajian, 1975; Thompson & Roberson, 1976). These techniques can be categorized based on the underlying approach (empirical, momentum-based, roughness height based, etc.) and applicable vegetation conditions (emergent, submerged, rigid, flexible, etc.) (Nepf, 2012). However, most of the approaches ultimately rely upon descriptions of vegetation characteristics (plant density, height, Leaf Area Index [LAI], and drag coefficient) and hydraulic conditions (water depth and velocity).

The implementation of resistance equations depends on the availability of vegetation parameters, which can be estimated either in the field or using remotely sensed data. For field-based measurements, the vegetation height can be determined using a handheld hypsometer (Gillihan, 2013), using conventional forest inventory methods with poles or trigonometric transformations of distance and angle measurements (Sexton, Bax, Sigueira, Swenson, & Hensley, 2009), and using terrestrial laser scanning (TLS) (Bywater-Reyes, Diehl, Wilcox, 2018). Similarly, vegetation density can be determined by counting the number of stems and measuring the diameter for a specific area (Gillihan, 2013), using TLS (Manners, Schmidt, & Wheaton, 2013), and using a parallel photographic method (Delai, Kiss, & Nagy, 2018). LAI is determined directly in the field using active laser sensors (e.g., TLS) (Antonarakis, Richards, Brasington, & Muller, 2010) or passive optical sensors (Gillihan, 2013). The collection of data in the field is labor-intensive and not operationally practical for large areas (Andersen, Reutebuch, & McGaughey, 2006).

The recent advancements in technology have eased the process of quantification of vegetation parameters, providing an opportunity to utilize vegetation resistance equations more effectively in hydraulic analysis at the reach scale. Remotely sensed data provide benefits over field-based methods with respect to data collection efficiency, spatial extent, and spatial resolution (Breda, 2003; Chen, McDermid,

Castilla, & Linke, 2017). Airborne light detection and ranging (LiDAR) data are widely used in forestry for determining vegetation height (Li et al., 2016; Sullivan, Ducey, Orwig, Cook, & Palace, 2017), LAI (Richardson, Moskal, & Kim, 2009; Solberg, Næsset, Hanssen, & Christiansen, 2006; Tseng, Lin, & Wang, 2016), phenology, and classification (Tomsett & Leyland, 2019). Some studies have utilized LiDAR to characterize vegetation and implement resistance equations to calculate vegetation-induced roughness (Abu-Aly et al., 2014; Antonarakis et al., 2010; Antonarakis, Richards, Brasington, Bithell, & Muller, 2008; Casas, Lane, Yu, & Benito, 2010; Mason, Cobby, Horritt, & Bates, 2003; Prior, Aquilina, Czuba, Pingel, & Hession, 2021; Straatsma & Baptist, 2008; Wang & Zhang, 2019). However, limited studies have explored the use of remotely sensed data to determine vegetation density in the context of hydraulic roughness (Straatsma, 2005; Straatsma & Baptist, 2008).

The incorporation of resistance relationships into hydrodynamic models for predicting the impacts of vegetation-induced roughness on flow characteristics is a topic of interest. Most studies using vegetation resistance equations used hypothetical or modeled water depth and velocity for non-vegetative conditions to calculate roughness (Abu-Aly et al., 2014; Delai et al., 2018; Wang & Zhang, 2019). Antonarakis et al. (2008) and (2010) used the allometric method to estimate the vegetation parameters and applied the drag-based resistance equations to determine roughness due to the stem and leafy structure of woody vegetation, respectively. Delai et al. (2018) used the method of Petryk and Bosmajian (1975) to estimate roughness due to vegetation in comparison to traditional constant roughness. Abu-Aly et al. (2014) determined roughness following the approach of Katul, Wiberg, Albertson, and Hornberger (2002). They used the water depth obtained from an unvegetated 2D hydrodynamic model (Sedimentation and River Hydraulics [SRH-2D]) to create the modified roughness map in post-processing. Similarly, Mason et al. (2003) and Prior et al. (2021) followed the approach of Fathi-Maghadam and Kouwen (1997) to determine vegetation height using LiDAR and drone-based laser scanning, respectively, to create the roughness map in post-processing. Straatsma and Baptist (2008) and Wang and Zhang (2019) calculated the roughness directly within the hydraulic model coupled with resistance equations. Straatsma and Baptist (2008) assessed water depth using a 2D model (Delft3D) by applying the approach of Baptist et al. (2007) and Wang and Zhang (2019) compared roughness based on nine different methods for the San Joaquin River using a one-dimensional (1D) hydrodynamic model.

As described above, a handful of studies have represented hydraulic roughness using vegetation resistance equations that rely on user-defined inputs (water depth and velocity). However, most hydrodynamic models are designed to use constant roughness values, leading to consistent reliance on traditional approaches. The studies presented in the previous section were focused on improving user assigned roughness in the presence of vegetation and the representation of higher resolution spatial distribution of vegetation characteristics. However, such efforts of improved vegetation characterization are still limited by the hydraulic models governing equations of vegetation roughness. Additional research is required to incorporate

vegetation roughness equations into modeling platforms. The purpose of this study was to determine the depth and velocity-dependent roughness based on the vertical distribution of vegetation characteristics (vegetation height), reconfiguration of vegetation under the flow (LAI and stem density), and spatial distribution based on the heterogeneity in vegetation species in floodplains following the equations proposed by Järvelä (2004) and Baptist et al. (2007). Further, very few studies have incorporated vegetation height and density into the analyses at the reach scale. There is a need to advance field-based and remotely sensed approaches for characterizing vegetation in resistance equations. The goal of this research was to develop, demonstrate, and evaluate a method for modeling hydraulic roughness in the presence of riparian vegetation. The research objectives were to (1) implement numerical routines for simulating vegetation-induced hydraulic roughness in a 2D hydrodynamic model; (2) evaluate the performance of two vegetation roughness approaches as compared with field measurements and the standard user assigned approach; and (3) compare vegetation parameters and hydrodynamic model results based on field-based and remote sensing acquisition methods.

#### 2 | METHODS

## 2.1 | Hydrodynamic model

In this study, the SRH-2D model developed by the United States Bureau of Reclamation (BOR) was used because this model is coupled with vegetation roughness routines to determine vegetation-induced roughness. The SRH-2D model simulates flow hydraulics in open channel river systems by solving the two-dimensional, depth-averaged dynamic wave equations, also known as the St. Venant equations (Lai, 2010). Within SRH-2D, hydraulic resistance is represented via descriptions of bed shear stresses ( $\tau_{\rm b}$ ) (Equations (1) and (2)).

$$\begin{pmatrix} \tau_{bx} \\ \tau_{by} \end{pmatrix} = \rho C_f \begin{pmatrix} U \\ V \end{pmatrix} \sqrt{U^2 + V^2}$$
 (1)

$$C_f = \frac{gn^2}{h^{1/3}} \tag{2}$$

where  $\rho$  is the water density,  $C_f$  is a roughness coefficient, U and V are the velocity magnitudes in the x (east/west) and y (north/south) coordinates, g is the acceleration due to gravity, and h is the flow depth. Roughness n is a user-specified parameter that generally does not change with flow conditions but can be spatially distributed depending on bed material and land cover (Lai, 2010).

The SRH-2D source code was modified (referred to as SRH-2DV) to calculate vegetation-induced roughness based on the equations proposed by Järvelä (2004) (Järvelä hereafter) and Baptist et al. (2007) (Baptist hereafter), to calculate floodplain roughness imparted by vegetation. These two resistance equations were selected because the required input vegetation parameters can readily be measured in the field and can also be extracted from LiDAR data. Within the SRH-2DV

model, the roughness value was partitioned into the roughness due to riparian vegetation  $(n_v)$  and grain roughness  $(n_o)$  to calculate the total roughness  $(n_t)$  (Dombroski, 2017). Hereafter, the roughness calculated using these two approaches is referred to as iteratively computed (IC) roughness  $(n_{IC})$ .

## 2.1.1 | Järvelä approach

The Järvelä approach is based on descriptions of submerged or emergent, flexible, and woody vegetation. Equation (3) represents the roughness imparted by leafy woody vegetation used by Järvelä (2004).

$$f = 4C_{d\chi} LAI \left(\frac{U}{U_{\chi}}\right)^{\chi} \frac{h}{H}$$
 (3)

where f is the Darcy-Weisbach friction factor,  $C_{d\chi}$  is the species-specific drag coefficient proposed by Järvelä (2004), LAI is the leaf area index (defined as the ratio of the area of one side of leaf tissue to the unit ground area), U is the approach velocity,  $U_{\chi}$  is the reference velocity,  $\chi$  is a species-specific exponent, h is the flow depth, and H is the vegetation height. This form of the equation is used for the case of emergent vegetation. To incorporate the technique into SRH-2D, f is converted to f using Equation (4).

$$n = h^{\frac{1}{6}} \sqrt{\frac{f}{8g}} \tag{4}$$

The Järvelä approach requires parameters LAI, H,  $C_{dx}$ ,  $\chi$ , and  $U_{x}$  to be specified. LAI and H can be measured in the field or determined from LiDAR data.  $C_{d_{\chi}}$  and  $\chi$  are unitless values that were determined for this study based on prior work done by Fathi-Moghadam (1996) and are specific for different vegetation types. According to Fathi-Moghadam (1996),  $C_{dy}$  can range from 0.43 to 0.69, while values of  $\chi$  can range from -0.57 to -0.38. The vegetation for this study consists of a number of species for which these parameters have yet to be defined. For this study,  $C_{d\chi}$  was set to 0.5 and  $\chi$  was set to -0.45.  $U_{\nu}$  is based on the lowest velocity applied when determining the value of  $\chi$  in the laboratory. In this study,  $U_{\chi}$  was set to 0.1 m/s (Järvelä, 2004). Hydraulic variables U and h are solved iteratively within the SRH-2DV model using depth average dynamic wave equations. These variables are first calculated based on user-defined default roughness and then iteratively solved in the presence of vegetation parameters.

## 2.1.2 | Baptist approach

The Baptist approach is based on a Chezy formulation, applicable to flow through submerged or emergent vegetation (Baptist et al., 2007). The computed resistance,  $C_{r_1}$  includes contributions from the bed,

vegetation, and boundary layer shear, where the vegetative drag is based on a cylindrical model (Equation (5)).

$$C_r = \sqrt{\frac{1}{\frac{1}{C_r^2} + \frac{(C_0 m D h)}{2g}}} + \frac{\sqrt{g}}{0.41} \log\left(\frac{h}{H}\right) \tag{5}$$

where  $C_b$  is the Chezy coefficient for the channel bed without vegetation,  $C_D$  is the drag coefficient for the vegetation type, m is the vegetation density specified as a number of stems per unit area, and D is the vegetation stem diameter. This form of the equation is used for the case of submerged vegetation. The second term on the right side of Equation (5) is set to zero for the case of emergent vegetation.  $C_r$  is converted to n using Equation (6).

$$n = \frac{1}{C_r} h^{\frac{1}{6}} \tag{6}$$

Application of the Baptist approach requires  $C_b$ ,  $C_D$ , D, H, and m to be specified prior to simulation.  $C_b$  and  $C_D$  are derived from previous studies (Baptist et al., 2007; Julien, 2002; Petryk & Bosmajian, 1975).  $C_b = 80$  was used in the evaluation of the model, and hence the contribution from bed roughness to the overall resistance is small. Determining C<sub>D</sub> requires both velocity and frontal area (Fischenich & Dudle, 1999), and is difficult to measure for natural vegetation in open channel flow. For flexible vegetation (willows), Wunder, Lehmann, and Nestmann (2011) found that  $C_D$  ranges from 0.35 to 0.85 in their laboratory experiment. However, Boothroyd, Hardy, Warburton, and Marjoribanks (2016) determined  $C_D$  as 1.24 and 1.54 for foliated and defoliated vegetation in the case of morphologically complex vegetation. A value of  $C_D = 1$  is often used for hydraulic analysis of vegetation (e.g., Baptist et al., 2007; Nehal, Yan, Xia, & Khaldi, 2012; Petryk & Bosmajian, 1975), which is used in this study as well for mixed vegetative conditions. D and H are measured in the field; the number of stems per transect (10 m  $\times$  10 m) is counted to estimate vegetation density (m). The hydraulic variable h is computed iteratively within the SRH-2DV model as mentioned in Section 2.1.1.

# 2.2 | Model application: San Joaquin River, California, USA

The model was applied and tested on a 20 km section of the San Joaquin River between Friant Dam and the Chowchilla Bifurcation, west of Fresno, California (Figure 1). This section was selected due to the presence of diverse riparian vegetation types and the availability of extensive field data, including measured water surface elevations (WSEs). Floodplain vegetation in the study reach was classified by Moise and Hendrickson (2002) using aerial imagery. They observed 11 types of vegetation based on Holland's system including cotton-wood riparian forest, herbaceous, mixed riparian forest, willow riparian forest, riparian oak forest, riparian scrub, river wash, wetland, willow scrub, exotic tree, and arundo (Holland, 1986).

FIGURE 1 Location of the study area along San Joaquin River in California, USA with the model boundary in dark shade

#### 2.3 | Vegetation parameters estimation

The two different methods (field measurements and LiDAR) were implemented to characterize vegetation and were then provided into the hydrodynamic model as the inputs to calculate hydraulic roughness. The SRH-2DV model for Järvelä and Baptist approach was simulated from these two data collection methods. The overview of the method is also outlined in the flow chart included in Appendix B (Figure B1).

## 2.3.1 | Field data

Field measurements were conducted in October 2012 to measure vegetation height, stem diameter, stem density, and LAI for each dominant vegetation class. Two to three field sites were identified to represent each of these vegetation classes. Vegetation characteristics were measured within a 10 m by 10 m transect (Bombino, Tamburino, & Zimbone, 2006; Kobziar & McBride, 2006; Wasser, Chasmer, Day, & Taylor, 2015) at each site. Vegetation height was measured with a hypsometer (Nikon Forestry Pro Laser) and stem diameter using measuring tape and caliper for smaller stems such as willows. The number of stems was counted to estimate the stem density in the transect. LAI was measured using a photosynthetically active radiation (PAR) sensor (Decagon AccuPAR model LP-80). A detailed description of the data collection activities, site photographs, and results can be found in Gillihan (2013).

#### 2.3.2 | LiDAR data

The LiDAR data used for the estimation of vegetation parameters were collected in 2015 (January 9 through February 11). The point cloud data were acquired at a flight altitude of 300 m above ground level. The density of collected data is an average of eight points per square meter. LiDAR data were processed in a standard GIS software package (ArcMap 10.6) to generate a Canopy Height Model (CHM), LAI, and density. The height of vegetation was represented using the

CHM (Mielcarek, Stereńczak, & Khosravipour, 2018). The modified Beer-Lambert equation (Bao et al., 2018; Kamoske, Dahlin, Stark, & Serbin, 2019; Richardson et al., 2009; Saitoh, Nagai, Noda, Muraoka, & Nasahara, 2012; Tseng et al., 2016), a widely used equation to determine the LAI of the forest canopy, was applied in this study to estimate LAI. The modified Beer-Lambert equation (Equation (7)) relates LAI to the number of ground points ( $N_g$ ), the number of total points ( $N_T$ ), and an extinction coefficient (k).

$$LAI = -\frac{1}{k} \ln \left( \frac{N_g}{N_T} \right) \tag{7}$$

k is given by 0.5/cos  $\theta$ , where  $\theta$  is the zenithal angle. The value of k is taken as 0.5 from the study of Richardson et al. (2009) because data were collected at the nadir angle. The detailed steps for finding vegetation height and LAI from LiDAR are documented in Chaulagain (2018).

Similarly, the density of vegetation was determined using the method developed by Straatsma (2005). Penetration Index (*PI*) was used to represent the density of vegetation from the LiDAR points represented by Equation (8). *PI* considers the stem density for vegetation height that a probable flood could inundate.

$$PI = \frac{1}{h_2 - h_1} \frac{N_{h_2 - h_1}}{N_{tot}}$$
 (8)

In this study,  $h_1$  was set to 0.30 m to avoid noise due to the ground surface (Straatsma & Baptist, 2008) and  $h_2$  was set to 3 m as the estimated depth of probable maximum vegetation inundation due to high flood events on a floodplain.  $N_{h2-h1}$  is the number of LiDAR points between  $h_1$  and  $h_2$ , where  $N_{tot}$  is the total number of points. The estimated density from PI represents the value (mD) given in Equation (5).

#### 2.4 | Model setup

The SRH-2D hydraulic model was originally developed and calibrated for the study reached by BOR to support a habitat restoration project

CHAULAGAIN ET AL.

(Reclamation, 2012). The computational mesh was generated using the surface-water modeling system software package (Aquaveo LLC, Provo, Utah). Floodplain topography was represented by the LiDARderived Digital Elevation Model with a spatial resolution of 1 m, collected in 2008. The river bathymetry was represented by the sound navigation and ranging data collected from 2009 to 2011 (Reclamation, 2012). The floodplain topography and river bathymetry were then interpolated to a 2D mesh. Quadrilateral mesh elements were used in-channel, while triangular elements were used within the floodplain. For irregular surfaces like the intersection between the main channel and floodplains and floodplains where an abrupt elevation change occurs, generally triangular mesh is used because it has more flexibility. In the river sections where flow is regular, the quadrilateral mesh is used. The average resolution of the 2D mesh was 9.5 m. Models were simulated for steady-state conditions. Steady discharge was used for upstream boundary conditions and WSEs were assigned for the downstream boundary as a function of the simulated discharges for model simulation.

#### 2.4.1 User assigned roughness model

The model was calibrated for four discharges (31, 71, 113, and 212 m<sup>3</sup>/s) because the floodplain starts to inundate when the flow exceeds 31 m<sup>3</sup>/s (Reclamation, 2012). The calibration was done by adjusting *n* values (without explicit consideration of vegetation) across the entire mesh to produce WSEs that closely matched observed WSEs in the field throughout the reach. For the context of this paper, the calibrated model is referred to as a *user assigned (UA) roughness (n)* model in which roughness is assigned by the user based on the traditional approach. A detailed description of model development, boundary conditions, and calibration of the model can be found in Gillihan (2013) and Reclamation (2012).

#### 2.4.2 | Iteratively computed roughness model

The SRH-2DV model was used for IC roughness calculation for the same 2D mesh and boundary conditions used for the calibrated model. For this study, the discharge of 113 and 212  $\rm m^3/s$  was only used by applying the Järvelä and Baptist approaches because there was less floodplain inundation for 31 and 71  $\rm m^3/s$ . The channel was defined with constant roughness of 0.035 and 0.025 for the open or bare land on a floodplain. The roughness for the floodplain covered with vegetation was computed as an IC roughness from the provided vegetation characteristic in the model.

To calculate IC roughness, the SRH-2DV model takes the input of vegetation parameters assigned based on land cover (vegetation mapping in geographic information system file format). Vegetation mapping is mapped to the computational 2D mesh by the vegetation module in the SRH-2DV model. Vegetation characteristics from field and LiDAR data were specified in each polygon. For the field method, vegetation parameters from 10 m  $\times$  10 m transects were extrapolated to other locations having the same vegetation species where

data was not collected (Gillihan, 2013). The vegetation parameters estimated from LiDAR were assigned by averaging the values of pixels that lie inside each polygon of vegetation mapping (Chaulagain, 2018) for each vegetation species. The default roughness based on the traditional approach was also provided in vegetation mapping, which is used to calculate the initial water depth and velocity for each mesh node. After that, the SRH-2DV model calculates IC roughness with internal iteration within a model based on the two vegetation parameters estimation method (field and LiDAR) and two resistance equations (Järvelä and Baptist) on each mesh element.

#### 2.5 | Sensitivity analysis

The parameters  $C_{d\chi}$ ,  $\chi$ , and  $C_D$  used in the roughness routines were based on those reported in previous literature and are species dependent. To understand the effect of these parameters on the flow depth, velocity, and overall  $n_{IC}$ , a sensitivity analysis was conducted. For Järvelä, both  $C_{d\chi}$  and  $\chi$  were independently increased and decreased by 0.1. For Baptist,  $C_D$  was increased or decreased by 0.5. The sensitivity analysis was performed for a flow rate of 113 m<sup>3</sup>/s.

#### 3 | RESULTS

### 3.1 | Model performance

The overall performance of the Järvelä and Baptist roughness routines was evaluated by comparing WSEs with directly measured WSEs in the field at two high discharges (113 and 212 m³/s). Table 1 summarizes the performance of the models based on the root mean square error (RMSE) calculated between models and measured WSEs for 113 and 212 m³/s. The UA model has lower RMSE compared to other models which was expected because this model was calibrated using the observed WSE data. RMSE values for all other models are lower than 0.5 m representing that all the models performed well in the presence of vegetation. Compared to all other models, Baptist-field has lower RMSE for both discharges representing better performance. Similarly, RMSE for the field-based method was smaller than the LiDAR-based method. Figure 2 includes the observed and simulated WSEs as a function of the channel station for a discharge of 212 m³/s. The pattern of the profile of simulated WSEs is similar to all

**TABLE 1** Summary of root mean square error (RMSE) (in meters) as a function of discharge for WSEs between all models compared to measured WSEs directly from the field

Discharge (m <sup>3</sup> /s)	113	212
User assigned	0.16	0.13
Järvelä-Field	0.12	0.26
Baptist-Field	0.18	0.16
Järvelä-LiDAR	0.37	0.48
Baptist-LiDAR	0.17	0.41

) on Wiley Online Library for rules of use; OA articles are governed by the applicable Creative Commons License

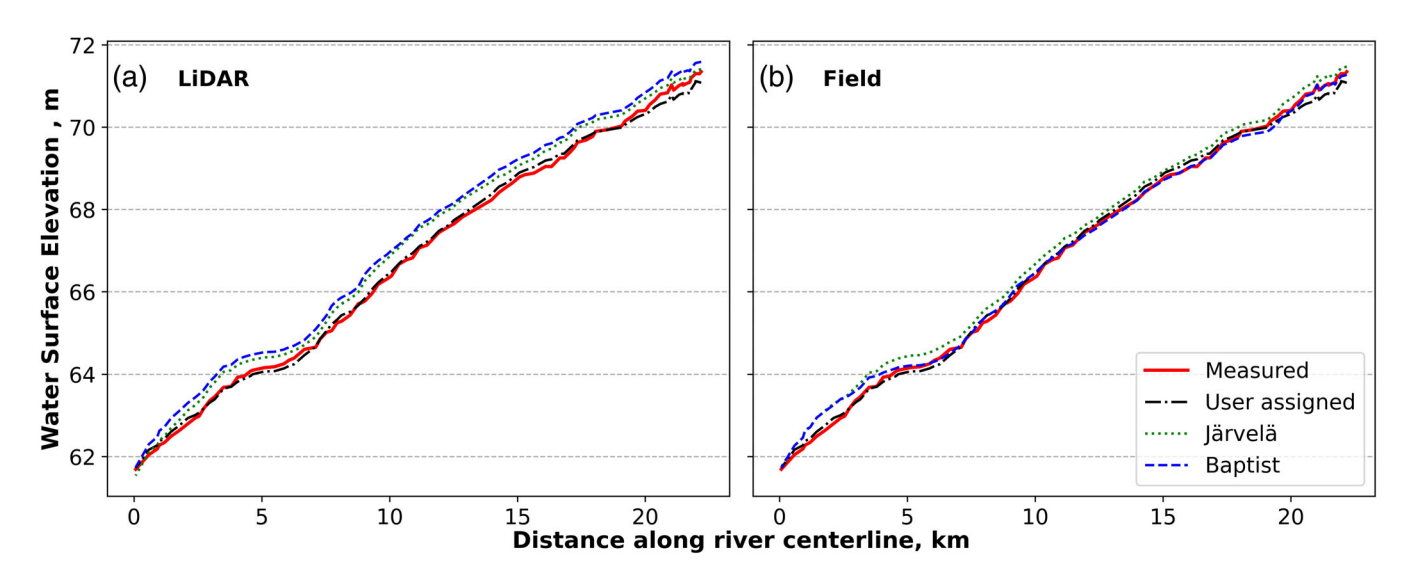


**FIGURE 2** WSEs along the river centerline for all models and measured WSE for 212 m<sup>3</sup>/s with vegetation parameters derived from (a) LiDAR-based data and (b) field-based data. (WSE: water surface elevation)

TABLE 2 Average value of vegetation parameters from the LiDAR and field-based methods (# refers to the number of stems)

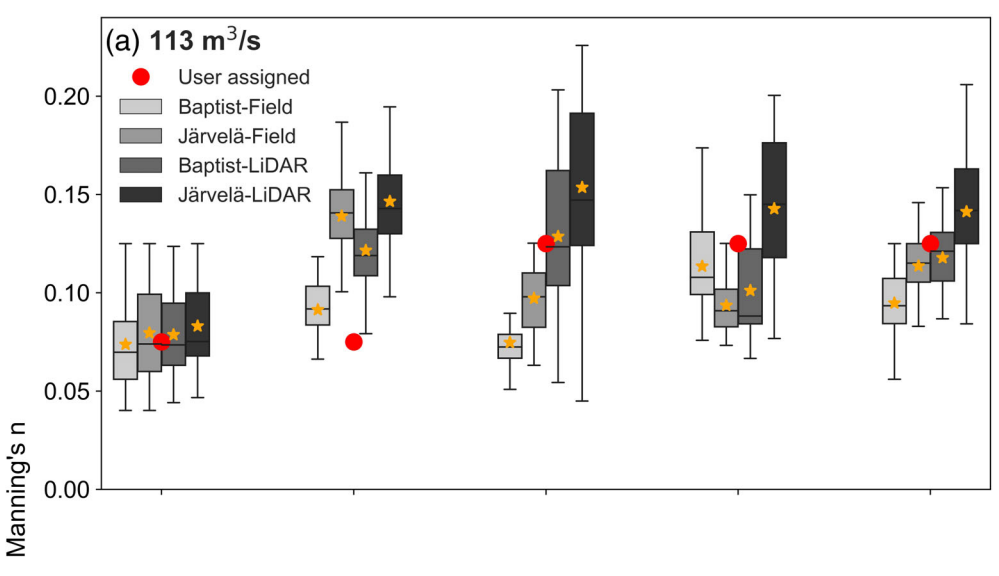
		LiDAR		Field			
Vegetation species	% Covered	Height (m)	LAI	Density (#/m²)	Height (m)	LAI	Density (#/m²)
Mixed riparian	19.55	6.12	3.01	0.1	8.60	2.33	0.04
Willow riparian	9.35	4.84	3.09	0.12	5.35	3.34	0.05
Herbaceous	9.20	1.26	0.82	0.03	0.92	0.05	0.004
Willow scrub	8.49	3.51	2.83	0.13	2.29	0.46	0.022
Cottonwood riparian low density	7.67	2.95	1.96	0.09	8.68	2.13	0.155
Agriculture field	7.05	1.69	0.69	0.05	2.20	0.08	0.016
Disturbed	5.39	-	-	-	-	-	-
Cottonwood riparian	4.25	6.46	2.79	0.1	4.36	2.88	0.017
Riparian scrub	3.54	2.33	1.77	0.08	0.79	0.48	0.018
River wash	3.29	-	-	-	-	-	-
Willow scrub low density	2.42	1.75	1.6	0.09	2.28	0.45	0.025
Exotic tree	1.43	11.40	2.43	0.05	5.41	3.42	0.05
Mixed riparian low density	1.37	4.18	2.3	0.09	2.20	0.08	0.016
Wetland/marsh	0.39	3.07	2.22	0.11	2.20	0.08	0.016
Arundo	0.09	6.15	2.18	0.13	4.60	3.04	0.017
Willow riparian low density	0.03	3.49	2.95	0.13	3.65	0.96	0.05

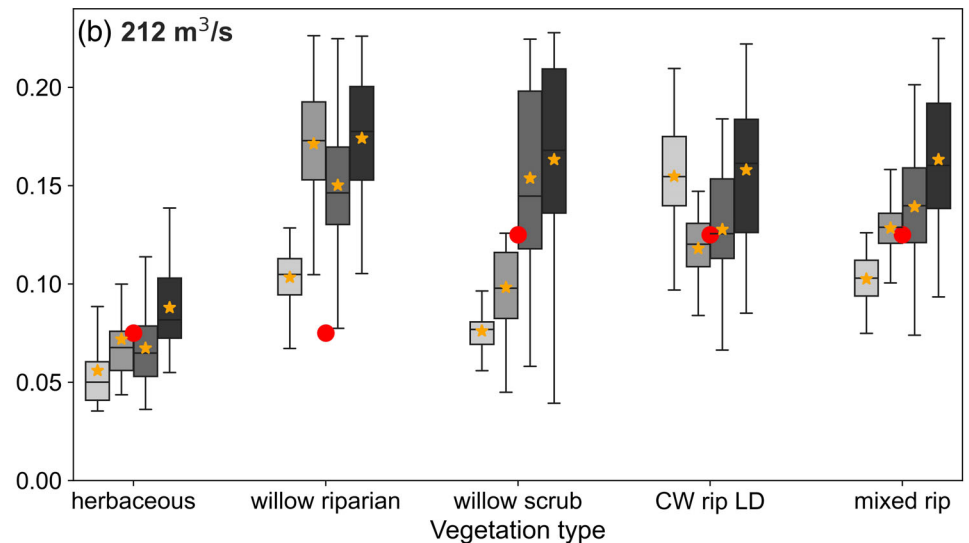
roughness modeling approaches. Within the IC roughness approaches, the Baptist field provided the closest match to field measurements along the study reach, but all other  $n_{IC}$  models overpredicted the WSEs.

## 3.2 | Vegetation parameters

The field- and LiDAR-based vegetation parameters were compared for different vegetation types (Table 2). The LiDAR method generally overpredicted the average vegetation height, LAI, and stem density for most vegetation species by 0.4, 0.77, and  $0.06/m^2$ , respectively, compared to the field data. The average vegetation height, LAI, and stem density range from 1.26 m (herbaceous) to 11.4 m (exotic), 0.69 (agriculture) to 3.09 (willow riparian), and 0.03 (herbaceous)/ $m^2$  to 0.13 (willow scrub, arundo, and willow riparian low density), respectively, from LiDAR data. From field data, the average vegetation height ranges from 0.92 m (herbaceous) to 8.68 m (cottonwood low density), LAI ranges from 0.05 (herbaceous) to 3.42 (exotic tree), and vegetation stem density ranges from 0.004 (herbaceous) to 0.155/ $m^2$  (cottonwood riparian low density).

FIGURE 3 Manning's n for the five most common vegetation types for discharges: (a) 113 m<sup>3</sup>/s and (b) 212 m<sup>3</sup>/s. Red dots represent the user assigned n. Star represents the mean iteratively computed roughness. The box height ranges between the 25% guartile (Q1) and 75% quartile (Q2), the solid middle line represents the median value, and the whiskers represent the minimum (Q1 - 1.5\*Inter Quartile Range [IQR]) and maximum value (Q2 + 1.5\*IQR). (CW rip LD: Cottonwood riparian low density and mixed rip: mixed riparian)





#### 3.3 | Impact of vegetation species on roughness

The  $n_{IC}$  varied as a function of vegetation species, modeling approach, and discharge (Figure 3). The box-whisker plots represent the roughness values for each vegetation polygon for the five most common vegetation types that were inundated at the discharge of 113 and 212 m³/s. The roughness values for all vegetation types are included in Tables A1 and A2 (Appendix A). The n value ranged from 0.056 to 0.125 for the calibrated model. The  $n_{IC}$  ranged from approximately 0.02 to 0.225 for both discharges. However, the mean  $n_{IC}$  was higher for all modeling approaches under the higher discharge condition. The box-whisker plot shows that IC roughness varies based on the modeling approaches, discharges, and vegetation types. For example, for all modeling approaches, IC roughness for herbaceous vegetation species ranges from 0.04 to 0.12 for 113 m³/s. For 212 m³/s, the ranges varied from 0.04 to 0.15 between the modeling approaches. The herbaceous vegetation has lower IC roughness compared to willow riparian

even though these two vegetation types were assigned with the same UA roughness for the calibrated model.

## 3.4 | Impact of vegetation on hydrodynamic results

The results revealed the variation in IC roughness associated with the spatial distribution of vegetation influencing the hydraulic parameters (water depth and velocity). The example of the spatial distribution of n and  $n_{IC}$  values is shown in Figure 4 for 212 m³/s, for an approximately 0.5 km sub-section of the study reach. The n values (Figure 4a) were specified by the modeler during calibration which does not change with discharge. The results shown in Figure 4b-e represent the  $n_{IC}$  values calculated via Järvelä and Baptist approaches for field and LiDAR methods. Considerable spatial variability was observed in  $n_{IC}$  values. That is,  $n_{IC}$  was different even for the same vegetation

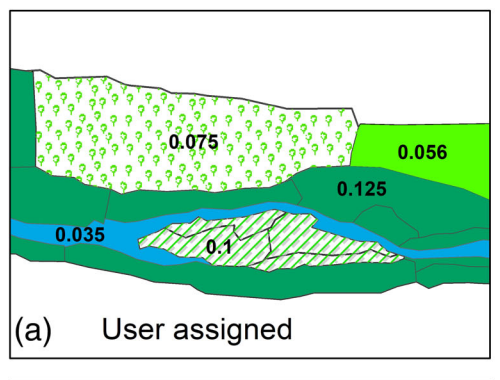
5351467, 2022, 10, Downloaded from https:

://onlinelibrary.wiley.com/doi/10.1002/rra.4053 by University

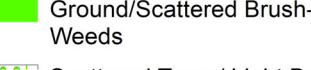
Of New Mexico, Wiley Online Library on [12/12/2022].

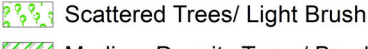
See the Terms

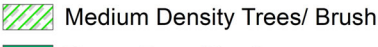
on Wiley Online Library for rules of use; OA articles are governed by the applicable Creative Commons











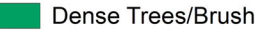
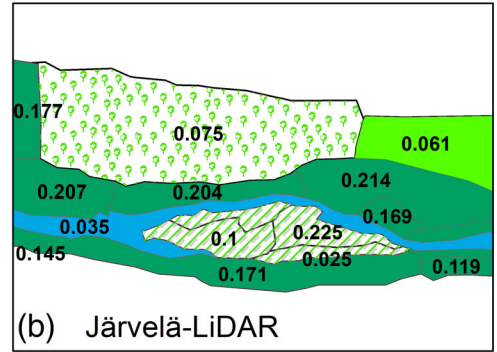
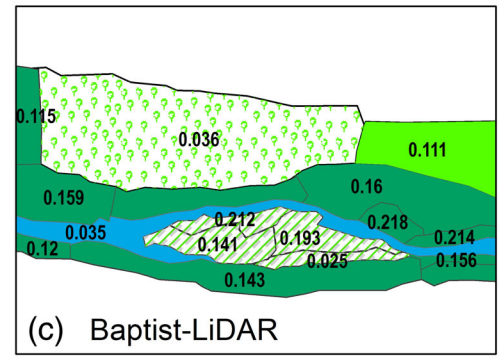


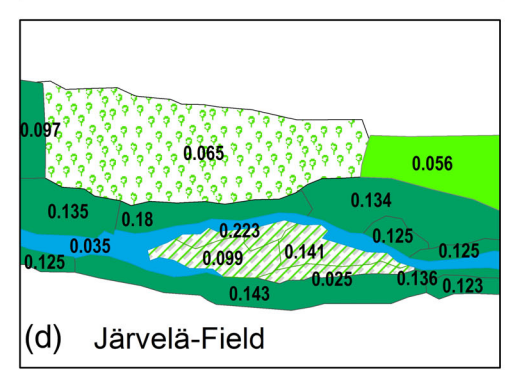


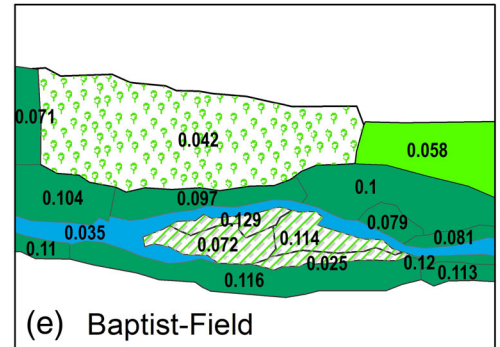


FIGURE 4 Average Manning's n based on land cover for 212 m<sup>3</sup>/s; (a) user assigned method, (b) Järvelä-LiDAR method. (c) Baptist-LiDAR method (d) Järvelä-Field method, and (e) Baptist-Field method









species under the same discharge depending on the modeling approach. For example, land cover represented by scattered trees is assigned with 0.075 UA roughness and IC roughness varies from 0.036 to 0.075 based on modeling approaches.

To investigate the variations of roughness as a function of the vegetation algorithm and parametrization approach, each of the IC roughness model outputs was compared to the calibrated UA model. The difference in velocity magnitude between n and  $n_{IC}$  models ( $\Delta V$ ) is shown in Figure 5 for the 212 m<sup>3</sup>/s. A positive value represents an area where the  $n_{IC}$  approach predicted a higher velocity than the n model and vice versa. For all conditions, the  $\Delta V$  was within  $\pm 0.5$  m/ s. For the readers' reference, the spatial distribution of water velocity magnitudes from all modeling approaches for 212 m<sup>3</sup>/s is shown in Figure B2 (Appendix B). Figures 4, 5, and B2 can be combined to investigate each polygon individually to understand the interactions between n values and velocity magnitude. For example, the  $n_{IC}$ approaches predicted lower roughness values than the n approach for the scattered trees vegetation type and higher values for the scattered brush-weeds vegetation type. The velocity magnitude changed

accordingly, with positive  $\Delta V$  reported in the areas of scattered trees and negative  $\Delta V$  for scattered brush weeds.

#### 3.5 Reach scale variation

The mean differences in the roughness  $(\Delta n_m)$ , velocity magnitude  $(\Delta V_m)$ , and water depth  $(\Delta d_m)$  for the IC models in comparison to the UA models for both discharges are summarized in Table 3. Here, positive values mean the IC model overpredicted values compared to the UA model. Overall, there were considerable changes (as high as  $\pm 0.03$ ) in  $n_{IC}$  compared to n. For most cases, the  $\Delta n_m$  was higher for LiDAR-based and lower for field-based approaches. In all cases, an inverse relationship was observed between  $\Delta n_m$  and  $\Delta V_m$  and a direct relationship between  $\Delta n_m$  and  $\Delta d_m$ . The two exceptions were found for the field-based IC roughness routines, but in both cases,  $\Delta n_m$ ,  $\Delta V_m$ , and  $\Delta d_m$  were relatively small.  $\Delta V_m$  was small throughout the reach, demonstrating that high- and low-velocity regions tended to cancel each out.

FIGURE 5 Difference in velocity for 212 m<sup>3</sup>/s between (a) user assigned and Järvela-LiDAR method, (b) user assigned and Baptist-LiDAR method. (c) user assigned and Järvelä-Field method, and (d) user assigned and Baptist-Field method. Positive values indicate the roughness routines overpredicted velocities relative to the user assigned model and vice versa. The line represents the land cover used for the user assigned roughness. The numerical value represents the roughness value based on each method

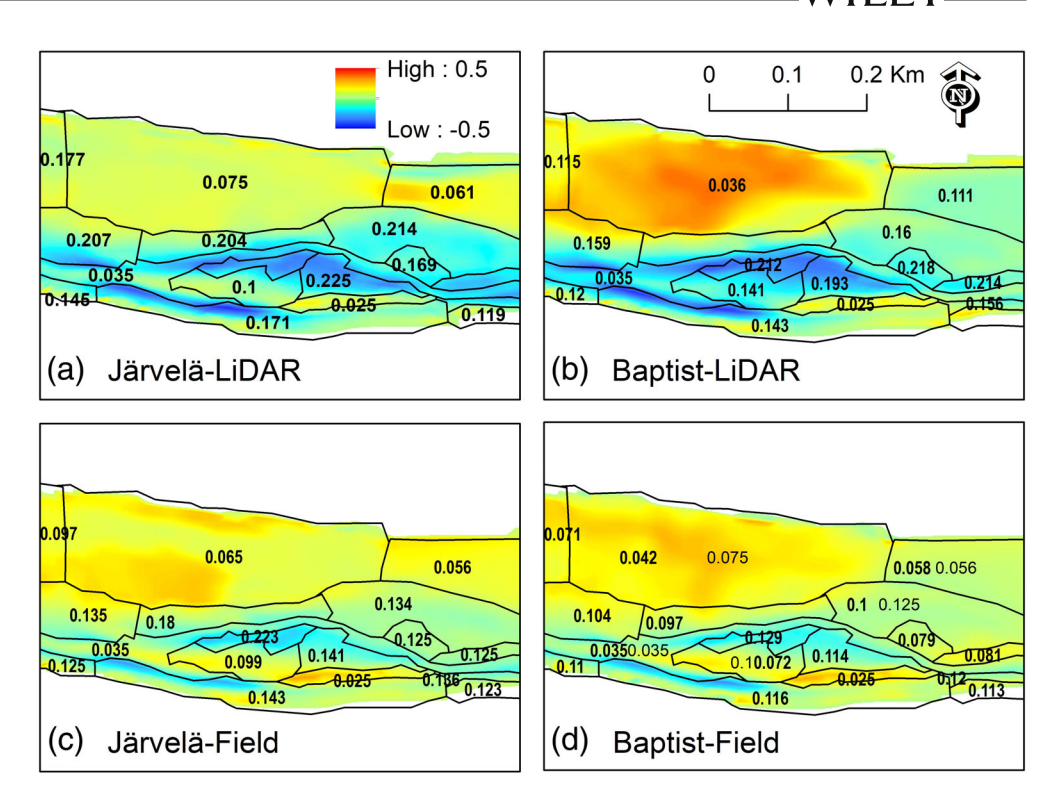


**TABLE 3** Mean differences in hydraulic parameters for the LiDAR- and field-based methods in relation to the user assigned roughness model for the Järvelä and Baptist approaches (positive values indicate higher values for iteratively computed roughness model as compared to user assigned roughness model and vice versa)

		LiDAR	LiDAR			Field		
Approach	Discharge (m <sup>3</sup> /s)	$\Delta n_{m}$	$\Delta V_{m}$ (m/s)	∆d <sub>m</sub> (m)	$\Delta n_{m}$	$\Delta V_{m}$ (m/s)	$\Delta d_{m}$ (m)	
Järvela	113	0.02	-0.03	0.36	-0.0002	0.003	0.13	
	212	0.03	-0.03	0.47	0.01	-0.005	0.24	
Baptist	113	0.001	-0.003	0.23	-0.02	0.03	-0.02	
	212	0.01	-0.01	0.39	-0.01	0.03	0.03	

Histograms were generated to provide more insight into the distribution in n, V, and d throughout the reach for 113 and 212 m<sup>3</sup>/s (Figure 6). The histogram represents the n, V, and d distributions for the percentage of wetted computational cells during simulation for the full model domain. The wetted cells for the channel were not included in the histograms because a constant Manning's n was assigned for all models. The histogram reveals a wider range in  $n_{IC}$ values (0.025-0.225) as compared to n values (0.056-0.125). The LiDAR-based Järvelä approach, for example, predicted a wide range of  $n_{IC}$  values with a large number of cells reporting values above 0.15. As a result, the velocity distributions tended to be low and the depth distribution was high. On the other hand, the field-based Baptist also produced a wider  $n_{IC}$  distribution than the n approach. The mean  $n_{IC}$ value was smaller by 0.001 than the n value, producing a small decrease in mean V by 1 cm/s and a reduction in d by 23 cm compared to UA roughness models (Table 3). Overall, the LiDAR-based methods tended toward higher predictions for roughness and water depth and lower predictions for velocity than the field-based and UA

modeling approaches. The discrepancies between modeling approaches increased as a function of discharge.

#### 3.6 | Sensitivity analysis

The required input parameters for the Järvelä and Baptist approaches can be categorized into data that can be gathered directly in the field or estimated from remote sensing data (e.g., stem density, LAI, and height) and parameters that are derived through lab experiments or from the literature (e.g.,  $C_{d\chi}$ ,  $\chi$ , and  $C_d$ ). Uncertainties exist in both parameter types that affect the model performance. However, much greater uncertainty is associated with the parameters that cannot be measured directly. Thus, a sensitivity analysis was conducted to investigate the influence of parameter uncertainties on model performance. The results of the sensitivity analysis were evaluated by comparing changes in the RMSE between simulated and measured WSEs for 113 m³/s as summarized in Table 4. Both the Järvelä and Baptist

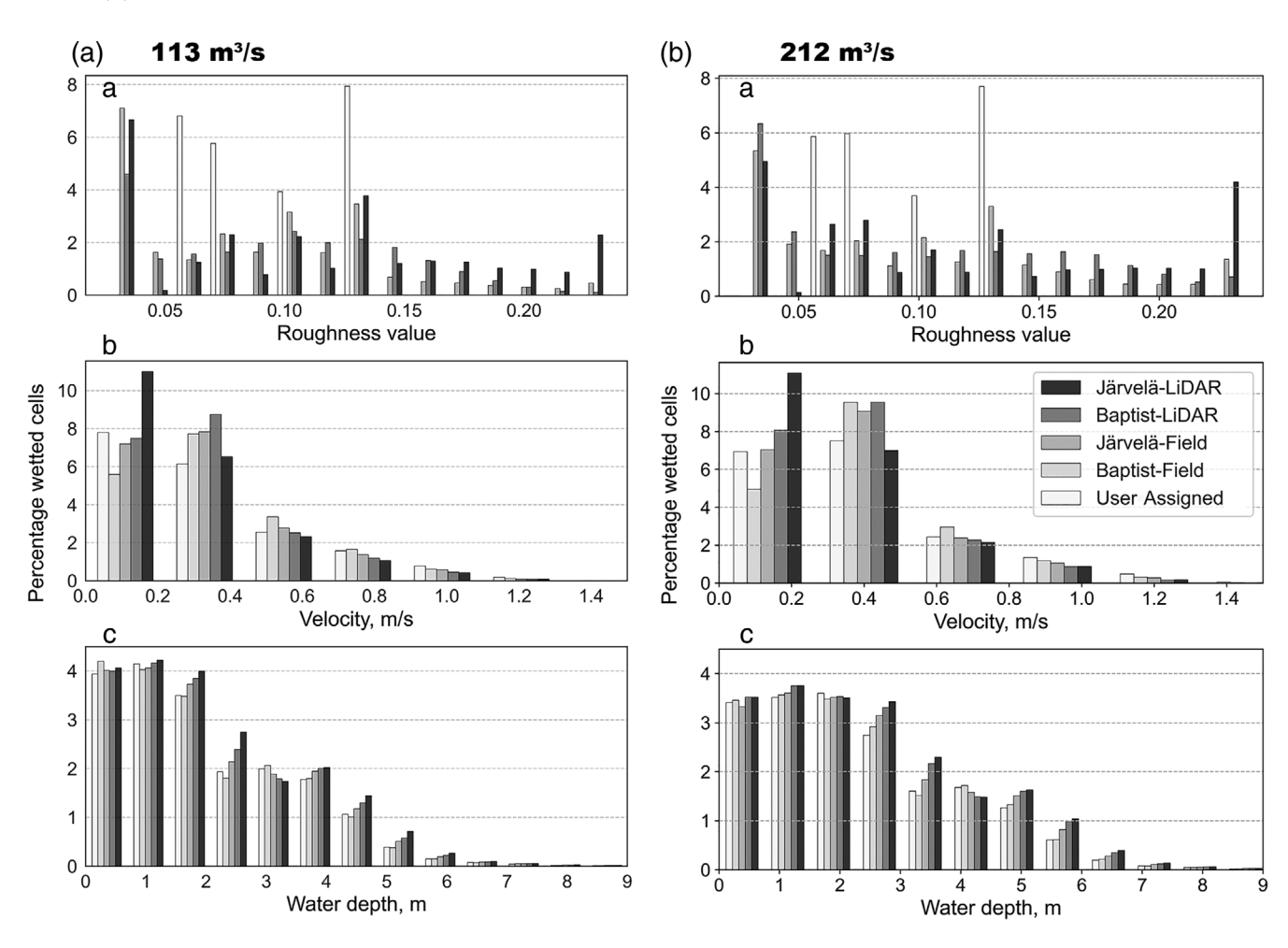


**FIGURE 6** Histogram plots for discharges: (i) 113 m<sup>3</sup>/s: (a). roughness value, (b). velocity, and (c) water depth and (ii) 212 m<sup>3</sup>/s: (a) roughness value, (b) velocity, and (c) water depth. The y-axis represents the percentage of wetted cells

**TABLE 4** Root mean square error (RMSE) for sensitivity analysis of WSEs for the Järvelä and the Baptist approaches using LiDAR- and Field-based method for  $113~\text{m}^3/\text{s}$  compared to measured WSEs directly from the field

	Parameters	LiDAR (m)	Field (m)
Järvelä	$C_{d\chi}=0.4,\chi=-0.35$	0.27	0.11
	$C_{d\chi}=0.4,\chi=-0.45$	0.24	0.11
	$C_{d\chi}=0.4,\chi=-0.55$	0.2	0.12
	$C_{d\chi}=0.5,\chi=-0.3$	0.33	0.15
	$C_{d\chi}=0.5, \chi=-0.35$	0.24	0.14
	$^aC_{d\chi}=0.5,\chi=-0.45$	0.37	0.12
	$C_{d\chi}=0.5,\chi=-0.55$	0.27	0.11
	$C_{d\chi}=0.6, \chi=-0.45$	0.32	0.14
Baptist	$C_d = 0.5$	0.12	0.28
	${}^{a}C_{d}=1$	0.18	0.17
	$C_d = 1.5$	0.29	0.14

 $<sup>{}^{\</sup>mathrm{a}}\mathrm{Represents}$  the parameters that were used for all other analyses in this study.

approaches were observed to be sensitive to the changes in input parameters. The RMSE values were less than 0.4 and 0.3 m for LiDAR- and field-based methods, respectively. For the Järvelä approach, the model was sensitive while increasing or decreasing  $C_{d\chi}$  keeping the  $\chi$  constant for both LiDAR- and field-based methods. Similarly, WSE was sensitive while changing  $C_D$  for the Baptist approach. The mean differences in hydraulic parameters while changing these parameters are summarized in Table A3 (Appendix A).

#### 4 | DISCUSSION

The evaluation of WSEs provided an integrated view of the hydrodynamic results, including insight into the models' ability to describe general flow characteristics along the streamwise coordinates. Although greater insight could be gained through a comparison of measured distributed hydraulic parameters (depth, velocity, and inundation area), such data are rarely available for high flows – as was the case for this study. Thus, the calibrated model was used to provide a

comparison with the status quo approach. This study has shown that both LiDAR and field methods yielded acceptable overall results (Figure 2) compared to the measured WSEs. Baptist-field outperformed all other approaches. This could be caused by the underestimation of vegetation stem density from field data. Overall, the LiDAR method estimated higher roughness values, which can be improved by collecting higher spatial resolution LiDAR data and through improved parameterization of vegetation characteristics.

In this study, LiDAR-derived IC roughness was higher than the field-based, especially for LiDAR-Järvelä. It signifies that  $n_{IC}$  could be improved by tuning up the parameters used in the Järvelä-LiDAR method. Some other studies (Antonarakis et al., 2008; Antonarakis et al., 2010) also estimated higher  $n_{IC}$  compared to n using the dragbased approach. The maximum  $n_{IC}$  values for cottonwood and exotic trees yielded by the Baptist approach also are higher (Tables A1 and A2). This is reasonable because the Baptist approach uses stem density, whereas the Järvelä approach uses LAI to represent the density of the vegetation. These results demonstrate that a specific approach's appropriateness depends on the vegetation's spatial characteristics. The selection of the approach also depends on the efficiency of estimation of vegetation parameters, vegetation species, and the corresponding parameters used in the equations. As such, the Järvelä approach is more appropriate to use in areas of high-density, leafy vegetation due to LAI being the controlling factor in these areas. The Baptist approach is better suited for areas of low vegetation density, where stem density dominates the flow resistance.

The accuracy in estimating vegetation-induced roughness also depends on the parameters used in the equations. For Järvelä, defining  $C_{d_{\chi}}$  and  $\chi$  is uncertain due to the limited research on these variables (Fathi-Moghadam, 1996). For Baptist, determining  $C_D$  is difficult due to the requirement of velocity and geometric measurements of the vegetation. Using a single value of  $C_D$  to represent all stems is often successfully practiced (Baptist et al., 2007; Nehal et al., 2012; Petryk & Bosmajian, 1975). All of the parameters depend on the species or class of vegetation. Few studies have been done to estimate those parameters for the wide range of potential riparian vegetation. A unique value for each vegetation class would likely increase accuracy. Most of the approaches have been tested for artificial plants in laboratory settings. For this particular model, approaches are defined on each polygon based on vegetated (categorized based on vegetation species) and non-vegetated polygons from vegetation mapping. Hence, the general modeling approach used in this study could accommodate the use of different approaches (Järvelä and Baptist) based on the vegetation species. Future modeling could be improved by including a combination of Järvelä and Baptist approaches based on the most suitable method for a given vegetation type.

The vegetation parameters and hydraulic variables influence the estimation of vegetation-induced roughness. The vegetation parameters such as height, LAI, and density measured from the field were lower than estimated using the LiDAR method. Several other studies (Breda, 2003; Richardson et al., 2009) also found that field-based characterization of vegetation parameters, such as height, LAI, and density, underpredicts those values compared to the LiDAR method.

In this study, the vegetation parameters were collected from a handful of 10 m  $\times$  10 m transects in the field and were then extrapolated to other locations. The representation of vegetation parameters from the field for a limited number of sites does not represent the true condition of spatially heterogeneous vegetation. For the same species of vegetation, the characteristics can differ substantially from those measured at random locations (Table 2). For larger study areas, collecting data from the entire study area is time-consuming and cost-prohibitive. However, even limited data from the field is valuable to groundtruth remotely sensed data. When applying vegetation-induced roughness approaches, using two distinct data sources allows the modeler to critically evaluate the model results through various methods rather than blindly trusting the data and results from a specific technique. It is advised that practitioners ground-truth any remotely observed data to a sub-portion of data that is directly observed. If there is no field data, conservative approaches such as comparing the remote sensing data with other reliable data sources can be performed.

Several limitations are present when estimating the vegetation parameters using the LiDAR method. The accuracy of parameters depends on the accuracy of LiDAR data. The vertical accuracy of the LiDAR data used in this study was ±13 cm at 95% confidence. The accuracy of vegetation height can be marginally improved by bias correction (Fradette, Leboeuf, Riopel, & Bégin, 2019). Similarly, several other studies (Bao et al., 2018; Kamoske et al., 2019; Richardson et al., 2009; Tseng et al., 2016) have experimented to improve the LAI using remote sensing approaches. The modified Beer-Lambert law used here to estimate LAI also introduces uncertainties related to k, which depends on the vegetation species and zenithal angle. LAI values can be improved by adjusting this k value. But in this study, to reduce the complexity and to test the effectiveness of the method for estimation of LAI as mentioned in the literature (Richardson et al., 2009), a single value was used to represent k for all vegetation types. Also, most of the methods used to determine LAI were developed in either dense forest canopy or crops, which are not the same as riparian vegetation. The estimation of stem density using LiDAR is rare. Straatsma and Baptist (2008) used LiDAR data collected for winter (leafless condition) to represent the density of riparian vegetation. In our study, we used the same LiDAR data collected in January through February (leaf-off season), to determine LAI and density of vegetation, whereas field data were collected in October (leaf-on season), which is another limitation related to data. LAI for the leaf-on season would be different depending on the season of data collection which would affect the estimation of roughness (Jalonen, Järvelä, & Aberle, 2013). The accuracy can also be improved using the higherdensity LiDAR points. In recent years, unmanned aircraft (e.g., drones) are gaining attention to collect higher spatial resolution LiDAR, which is cheaper than manned aircraft for data collection.

In our study, we found that  $n_{IC}$  was higher than n for LiDAR and lower for the field method for the study reach. However,  $n_{IC}$  showed a wider range (below or above the n) for the same land cover or vegetation types depending on the discharge (Figure 3), which was expected compared to the constant roughness given in the guidelines

of Arcement and Schneider. (1989). Also, n values are assigned in much lower resolution and represent an average value spatially on a per-polygon basis. However,  $n_{IC}$  values are calculated on a grid-cell basis (of the 2D mesh) considering the effect of hydraulic variables. This leads to  $n_{IC}$  having a higher spatial variability and a wider range of values, as shown in this study. Previous studies also showed a higher and wider range of  $n_{IC}$  values than standard references for riparian forests (Abu-Aly et al., 2014; Antonarakis et al., 2010; Delai et al., 2018). The result of this spatial diversity demonstrates that vegetation-induced roughness is usually higher, especially for dense vegetation compared to the UA roughness for the same vegetation type with high spatial heterogeneity.

The sensitivity analysis performed for Järvelä and Baptist approaches revealed the major influence of the parameters  $C_{d\chi}$ ,  $\chi$ , and  $C_D$ . The model results were more sensitive due to the change in  $C_{d\chi}$  for the Järvelä approach. It is because  $C_{d\chi}$  is dependent mainly on the vegetation species and using the single value for diverse vegetation conditions is likely to influence the model outputs. The experiment of Jalonen et al. (2013) also suggested that the relationship between the drag force  $C_{d\chi}$  and the velocity U is linear, correlating to a  $\chi$  value of -1 for all vegetation species and LAI is the controlling factor for the estimation of roughness. The models were sensitive while increasing or decreasing  $C_D$  for the Baptist approach. This study suggested that more research is needed to properly parametrize  $C_{d\chi}$ ,  $\chi$ , and  $C_D$  to improve the estimation of hydraulic roughness induced by riparian vegetation.

The presence of vegetation on the floodplain complicates the flow field by altering the velocity and water depth. In addition to hydraulic conditions, vegetation structure also affects ecological processes such as transferring nutrients and larvae (Stella, Rodríguez-González, Dufour, & Bendix, 2013). This study demonstrates how that hydraulic roughness varies as a function of spatial locations and discharge based on vegetation species. Therefore, it is recommended to describe roughness based on spatial locations and discharge for projects such as habitat restoration, side channel construction, bank stabilization, and so on. The ability to describe vegetation-induced roughness in detail enhances the understanding of hydraulics and ecological processes which provides beneficial information for making informed decisions for river management.

A 2D hydrodynamic model was tested for two resistance equations to determine the vegetation-induced hydraulic roughness. The approach could be easily implemented in other 2D numerical models (e.g., HEC-RAS 2D, TUFLOW, etc.) by customizing the source code. Furthermore, Järvelä and Baptist approaches performed well overall in the presence of vegetation even without calibration, which shows the method's applicability even if the field data is lacking. As mentioned before, calibration of remote sensing data with the field data for vegetation parameters is still recommended. This study has advanced the implementation of emerging technology (e.g., LiDAR) and novel methods to understand vegetation-induced roughness in reach and sub-reach scale models. The modeling approach used in this study has implications for a broader range of river systems.

#### 5 | CONCLUSION

The goal of this research was to develop, demonstrate, and evaluate a method for modeling hydraulic roughness in the presence of riparian vegetation. This was accomplished by implementing and evaluating two numerical routines for simulating roughness using both fieldbased and LiDAR-based data for parameterization. The simulation results also demonstrate the potential for using remote sensing data to characterize land cover and vegetation characteristics, which can be used to efficiently and consistently parameterize 2D hydrodynamic models. The parameterization methods demonstrate acceptable performance making the method suitable for modeling even if field data are lacking. The results show that the hydraulic roughness due to vegetation varies spatially in relation to vegetation species which are sensitive to hydraulic conditions (water depth and velocity). This directs toward the necessity of describing roughness in detail for sensitive projects such as habitat restoration, side channel construction, bank stabilization, and so on. The ability to describe detail roughness greatly enhances the understanding of the system, allowing for better planning and management. Both approaches discussed in this study are promising techniques for future hydraulic modeling. However, further investigation must be done to improve the accuracy of parameters (e.g., k for LAI) used for the estimation of vegetation characteristics from LiDAR data and the parameters ( $C_{d\chi}$ ,  $\chi$ , and  $C_D$ ) used in these approaches. It is recommended to perform a similar sensitivity analysis in future studies to investigate the possible range of outcomes. It is also suggested to collect LiDAR and field data in the same season for a better comparison of vegetation parameters to improve the estimation of roughness. It also shows that the field data holds great significance in the ground-truthing of remotely sensed data for the estimation of vegetation characteristics. Unmanned aircraft-based LiDAR can be implemented to collect the high spatial resolution LiDAR to improve the estimation of vegetation parameters. The approach used here can be readily implemented in other study areas based on data availability. Overall, this study demonstrated a novel approach for advancing techniques and software to improve hydrodynamic model performance in the presence of vegetation.

#### **ACKNOWLEDGMENTS**

We would like to acknowledge funding from the National Science Foundation (Awards #1254569 and #1641289) to accomplish this research. We would also like to thank the Bureau of Reclamation Technical Services Center for providing the necessary data and access to the model to complete this research.

#### **CONFLICT OF INTEREST**

The authors declare that there is no conflict of interest.

#### **DATA AVAILABILITY STATEMENT**

All the data used in this research is from the U.S. Bureau of Reclamation, Denver, Colorado, USA. The data that support the findings of this study are available from the corresponding author, upon request.

#### REFERENCES

- Abu-Aly, T. R., Pasternack, G. B., Wyrick, J. R., Barker, R., Massa, D., & Johnson, T. (2014). Effects of LiDAR-derived, spatially distributed vegetation roughness on two-dimensional hydraulics in a gravel-cobble river at flows of 0.2 to 20 times bankfull. *Geomorphology*, 206, 468–482. https://doi.org/10.1016/j.geomorph.2013.10.017
- Andersen, H.-E., Reutebuch, S. E., & McGaughey, R. J. (2006). A rigorous assessment of tree height measurements obtained using airborne lidar and conventional field methods. *Canadian Journal of Remote Sensing*, 32(5), 355–366. https://doi.org/10.5589/m06-030
- Anderson, B. G., Rutherfurd, I. D., & Western, A. W. (2006). An analysis of the influence of riparian vegetation on the propagation of flood waves. *Environmental Modelling & Software*, 21(9), 1290–1296. https://doi. org/10.1016/j.envsoft.2005.04.027
- Antonarakis, A. S., Richards, K. S., Brasington, J., & Muller, E. (2010). Determining leaf area index and leafy tree roughness using terrestrial laser scanning: Terrestrial LiDAR and laser scanning. *Water Resources Research*, 46(6), W06510. https://doi.org/10.1029/2009WR008318
- Antonarakis, A. S., Richards, K. S., Brasington, J., Bithell, M., & Muller, E. (2008). Retrieval of vegetative fluid resistance terms for rigid stems using airborne lidar: Stem roughness using airborne LiDAR. *Journal of Geophysical Research Biogeosciences*, 113(G2), G02S07. https://doi.org/10.1029/2007JG000543
- Arcement, G. J., & Schneider, R. S. (1989). Guide for selecting Manning's roughness coefficients for natural channels and flood plains (FHWA-TS-84-204; water supply paper). U.S.D.T., Federal Highway Administration, Washington, D.C.
- Bao, Y., Ni, W., Wang, D., Yue, C., He, H., & Verbeeck, H. (2018). Effects of tree trunks on estimation of clumping index and lai from hemiview and terrestrial LiDAR. *Forests*, 9(3), 144. https://doi.org/10.3390/ f9030144
- Baptist, M. J., Babovic, V., Rodríguez Uthurburu, J., Keijzer, M., Uittenbogaard, R. E., Mynett, A., & Verwey, A. (2007). On inducing equations for vegetation resistance. *Journal of Hydraulic Research*, 45(4), 435–450. https://doi.org/10.1080/00221686.2007.9521778
- Bombino, G., Tamburino, V., & Zimbone, S. M. (2006). Assessment of the effects of check-dams on riparian vegetation in the mediterranean environment: A methodological approach and example application. *Ecological Engineering*, 27(2), 134–144. https://doi.org/10.1016/j.ecoleng.2006.01.005
- Boothroyd, R. J., Hardy, R. J., Warburton, J., & Marjoribanks, T. I. (2016). The importance of accurately representing submerged vegetation morphology in the numerical prediction of complex river flow. *Earth Surface Processes and Landforms*, 41(4), 567–576. https://doi.org/10.1002/esp.3871
- Brauman, K. A., Daily, G. C., Duarte, T. K., & Mooney, H. A. (2007). The nature and value of ecosystem services: An overview highlighting hydrologic services. Annual Review of Environment and Resources, 32(1), 67–98. https://doi.org/10.1146/annurev.energy.32.031306.102758
- Breda, N. J. J. (2003). Ground-based measurements of leaf area index: A review of methods, instruments and current controversies. *Journal of Experimental Botany*, 54(392), 2403–2417. https://doi.org/10.1093/jxb/erg263
- Butterfield, B. J., Grams, P. E., Durning, L. E., Hazel, J., Palmquist, E. C., Ralston, B. E., & Sankey, J. B. (2020). Associations between riparian plant morphological guilds and fluvial sediment dynamics along the regulated Colorado River in grand canyon. River Research and Applications, 36, 410-421.
- Byrne, C. F. (2017). A numerical investigation of the implications of altered channel-floodplain connectivity on hydrodynamic flood wave processes. PhD dissertation. New Mexico: University of New Mexico.
- Bywater-Reyes, S., Diehl, R. M., & Wilcox, A. C. (2018). The influence of a vegetated bar on channel-bend flow dynamics. *Earth Surface Dynamics*, 6(2), 487–503. https://doi.org/10.5194/esurf-6-487-2018
- Carollo, F. G., Ferro, V., & Termini, D. (2005). Flow resistance law in channels with flexible submerged vegetation. *Journal of Hydraulic*

- Engineering, 131(7), 554-564. https://doi.org/10.1061/(ASCE)0733-9429(2005)131:7(554)
- Casas, A., Lane, S. N., Yu, D., & Benito, G. (2010). A method for parameterising roughness and topographic sub-grid scale effects in hydraulic modelling from LiDAR data. *Hydrology and Earth System Sciences*, 14(8), 1567–1579. https://doi.org/10.5194/hess-14-1567-2010
- Chanson, H. (2004). Environmental hydraulics for open channel flows (1st ed.). Oxford: Elsevier Butterworth-Heinem.
- Chaulagain, S. (2018). An investigation into remote sensing techniques for describing hydraulic roughness. Master's thesis. New Mexico: University of new Mexico. https://digitalrepository.unm.edu/ce\_etds/210/
- Chen, S., McDermid, G. J., Castilla, G., & Linke, J. (2017). Measuring vegetation height in linear disturbances in the boreal Forest with UAV photogrammetry. *Remote Sensing*, 9(12), 1257. https://doi.org/10.3390/rs9121257
- Chow, V. T. (1959). Open-Channel hydraulics. New York: McGraw-Hill.
- Croke, J., Thompson, C., & Fryirs, K. (2017). Prioritising the placement of riparian vegetation to reduce flood risk and end-of-catchment sediment yields: Important considerations in hydrologically-variable regions. *Journal of Environmental Management*, 190, 9–19. https://doi.org/10.1016/j.jenvman.2016.12.046
- Curran, J. C., & Hession, W. C. (2013). Vegetative impacts on hydraulics and sediment processes across the fluvial system. *Journal of Hydrology*, 505, 364–376. https://doi.org/10.1016/j.jhydrol.2013.10.013
- Curran, J. H., & Wohl, E. E. (2003). Large woody debris and flow resistance in step-pool channels, Cascade Range, Washington. *Geomorphology*, 51(1-3), 141-157. https://doi.org/10.1016/S0169-555X(02)00333-1
- Darby, S. E. (1999). Effect of riparian vegetation on flow resistance and flood potential. 12.
- Delai, F., Kiss, T., & Nagy, J. (2018). Field-based estimates of floodplain roughness along the Tisza River (Hungary): The role of invasive Amorpha fruticosa. *Applied Geography*, 90, 96–105. https://doi.org/10.1016/j.apgeog.2017.11.006
- Dombroski, D. (2017). Remote sensing of vegetation characteristics for estimation of partitioned roughness in hydraulic and sediment transport modeling applications. Bureau of Reclamation, Denver technical service center, 6th Ave & Kipling St., PO Box 25007, Denver, CO 80225.
- Dosskey, M. G., Vidon, P., Gurwick, N. P., Allan, C. J., Duval, T. P., & Lowrance, R. (2010). The role of riparian vegetation in protecting and improving chemical water quality in streams. *JAWRA Journal of the American Water Resources Association*, 46(2), 261–277. https://doi.org/10.1111/j.1752-1688.2010.00419.x
- Dufour, S., & Rodríguez-González, P. M. (2019). Riparian zone / riparian vegetation definition: Principles and recommendations (p. 20). Belgium: COST Action CA16208 CONVERGES.
- Fathi-Maghadam, M., & Kouwen, N. (1997). Nonrigid, nonsubmerged, vegetative roughness on floodplains. *Journal of Hydraulic Engineering*, 123(1), 51–57. https://doi.org/10.1061/(ASCE)0733-9429(1997)123:1(51)
- Fathi-Moghadam, M. (1996). Momentum absorption in non-rigid, nonsubmerged, tall vegetation along rivers. PhD thesis. Waterloo: University of Waterloo.
- Fischenich, C., & Dudle, S. (1999). Determining Drag Coefficients and Area for vegetation. 14.
- Forzieri, G., Moser, G., Vivoni, E. R., Castelli, F., & Canovaro, F. (2010). Riparian vegetation mapping for hydraulic roughness estimation using very high resolution remote sensing data fusion. *Journal of Hydraulic Engineering*, 136(11), 855–867. https://doi.org/10.1061/(ASCE)HY. 1943-7900 0000254
- Fradette, M.-S., Leboeuf, A., Riopel, M., & Bégin, J. (2019). Method to reduce the bias on digital terrain model and canopy height model from LiDAR data. *Remote Sensing*, 11(7), 863. https://doi.org/10.3390/rs11070863
- Gillihan, T. (2013). Dynamic vegetation roughness in the riparian zone. New Mexico: University of New Mexico.
- Green, J. C. (2005). Modelling flow resistance in vegetated streams: Review and development of new theory. *Hydrological Processes*, 19(6), 1245–1259. https://doi.org/10.1002/hyp.5564



- Groffman, P. M., Bain, D. J., Band, L. E., Belt, K. T., Brush, G. S., Grove, J. M., ... Zipperer, W. C. (2003). Down by the riverside: Urban riparian ecology. Frontiers in Ecology and the Environment, 1(6), 315–321. https://doi.org/10.1890/1540-9295(2003)001[0315:DBTRUR]2. 0 CO:2
- Gurnell, A. (2014). Plants as river system engineers: Plants as river system engineers. Earth Surface Processes and Landforms, 39(1), 4–25. https://doi.org/10.1002/esp.3397
- Hamilton, S. K. (2012). Biogeochemical time lags may delay responses of streams to ecological restoration. Freshwater Biology, 57(s1), 43–57. https://doi.org/10.1111/j.1365-2427.2011.02685.x
- Hession, W. C., & Curran, J. C. (2013). The impacts of vegetation on roughness in fluvial systems. In J. Shroder, D. R. Butler & C. R. Hupp (Eds.), Treatise on geomorphology (pp. 75–93). San Diego, CA: Academic Press.
- Hicks, D. M., & Mason, P. D. (1991). Roughness characteristics of New Zealand rivers: A handbook for assigning hydraulic roughness coefficients to river reaches by the "visual comparison" approach. [Wellington, N.Z.]: Water resources survey, DSIR marine and freshwater. https:// trove.nla.gov.au/version/43111700
- Holland, R. F. (1986). Preliminary descriptions of the terrestrial natural communities of California. Sacramento, California: The Resources Agency Non-game Heritage Program Department of Fish and Game.
- Jalonen, J., Järvelä, J., & Aberle, J. (2013). Leaf area index as vegetation density measure for hydraulic analyses. *Journal of Hydraulic Engineer*ing, 139(5), 461–469. https://doi.org/10.1061/(ASCE)HY.1943-7900. 0000700
- Julien, P. Y. (2002). River mechanics. Cambridge, UK: Cambridge University press. https://doi.org/10.1017/9781316107072
- Järvelä, J. (2004). Determination of flow resistance caused by nonsubmerged woody vegetation. *International Journal of River Basin Man*agement, 2(1), 61–70. https://doi.org/10.1080/15715124.2004. 9635222
- Kamoske, A. G., Dahlin, K. M., Stark, S. C., & Serbin, S. P. (2019). Leaf area density from airborne LiDAR: Comparing sensors and resolutions in a temperate broadleaf forest ecosystem. Forest Ecology and Management, 433, 364–375. https://doi.org/10.1016/j.foreco.2018.11.017
- Katul, G., Wiberg, P., Albertson, J., & Hornberger, G. (2002). A mixing layer theory for flow resistance in shallow streams: Mixing layer theory for flow resistance. Water Resources Research, 38(11), 32-1–32-8. https:// doi.org/10.1029/2001WR000817
- Kim, J.-S. (2010). Roughness coefficient and its uncertainty in gravel-bed river. Water Science and Engineering, 3(2), 16.
- Kobziar, L. N., & McBride, J. R. (2006). Wildfire burn patterns and riparian vegetation response along two northern Sierra Nevada streams. Forest Ecology and Management, 222(1), 254–265. https://doi.org/10.1016/j. foreco.2005.10.024
- Kouwen, N., & Fathi Moghadam, M. (2000). Friction factors for coniferous trees along rivers. *Journal of Hydraulic Engineering ASCE*, 126, 732– 740. https://doi.org/10.1061/(ASCE)0733-9429(2000)126:10(732)
- Kouwen, N., & Li, R.-M. (1980). Biomechanics of vegetative channel linings. *Journal of the Hydraulics Division*, 106(6), 1085–1103.
- Lai, Y. G. (2010). Two-dimensional depth-averaged flow modeling with an unstructured hybrid mesh. *Journal of Hydraulic Engineering*, 136(1), 12–23. https://doi.org/10.1061/(ASCE)HY.1943-7900.0000134
- Lawrence, C. B., Pindilli, E. J., & Hogan, D. M. (2019). Valuation of the flood attenuation ecosystem service in difficult run, VA, USA. *Journal* of Environmental Management, 231, 1056–1064. https://doi.org/10. 1016/j.jenvman.2018.10.023
- Li, W., Niu, Z., Chen, H., Li, D., Wu, M., & Zhao, W. (2016). Remote estimation of canopy height and aboveground biomass of maize using high-resolution stereo images from a low-cost unmanned aerial vehicle system. *Ecological Indicators*, 67, 637–648. https://doi.org/10.1016/j.ecolind.2016.03.036
- Lightbody, A. F., & Nepf, H. M. (2006). Prediction of velocity profiles and longitudinal dispersion in salt marsh vegetation. *Limnology and Ocean-ography*, 51(1), 218–228. https://doi.org/10.4319/lo.2006.51.1.0218

- Manners, R., Schmidt, J., & Wheaton, J. M. (2013). Multiscalar model for the determination of spatially explicit riparian vegetation roughness. *Journal of Geophysical Research - Earth Surface*, 118(1), 65–83. https://doi.org/10.1029/2011JF002188
- Marcus, W. A., Roberts, K., Harvey, L., & Tackman, G. (1992). An evaluation of methods for estimating manning's n in small mountain streams. Mountain Research and Development, 12(3), 227. https://doi.org/10.2307/3673667
- Mason, D. C., Cobby, D. M., Horritt, M. S., & Bates, P. D. (2003). Floodplain friction parameterization in two-dimensional river flood models using vegetation heights derived from airborne scanning laser altimetry. *Hydrological Processes*, 17(9), 1711–1732. https://doi.org/10.1002/ hvp.1270
- Masterman, R., & Thorne, C. R. (1992). Predicting influence of bank vegetation on channel capacity. *Journal of Hydraulic Engineering*, 118(7), 1052–1058. https://doi.org/10.1061/(ASCE)0733-9429(1992)118:7 (1052)
- Mielcarek, M., Stereńczak, K., & Khosravipour, A. (2018). Testing and evaluating different LiDAR-derived canopy height model generation methods for tree height estimation. *International Journal of Applied Earth Observation and Geoinformation*, 71, 132–143. https://doi.org/10.1016/j.jag.2018.05.002
- Moise, G. W., & Hendrickson, B. (2002). *Riparian vegetation of the San Joaquin River*. California: Department of Water Resources San Joaquin District Environmental Services Section Fresno.
- Naiman, R. J., Decamps, H., & Pollock, M. (1993). The role of riparian corridors in maintaining regional biodiversity. *Ecological Applications*, 3(2), 209–212. https://doi.org/10.2307/1941822
- Nehal, L., Yan, Z. M., Xia, J. H., & Khaldi, A. (2012). Flow through nonsubmerged vegetation: A flume experiment with artificial vegetation.
- Nepf, H. M. (1999). Drag, turbulence, and diffusion in flow through emergent vegetation. Water Resources Research, 35(2), 479–489. https://doi.org/10.1029/1998WR900069
- Nepf, H. M. (2012). Flow and transport in regions with aquatic vegetation. Annual Review of Fluid Mechanics, 44, 123–142. https://doi.org/10. 1146/annurev-fluid-120710-101048
- Nepf, H., & Ghisalberti, M. (2008). Flow and transport in channels with submerged vegetation. *Acta Geophysica*, *56*(3), 753–777. https://doi.org/10.2478/s11600-008-0017-y
- Petryk, S., & Bosmajian, G. (1975). Analysis of flow through vegetation. *Journal of the Hydraulics Division*, 101(7), 871–884.
- Picco, L., Comiti, F., Mao, L., Tonon, A., & Lenzi, M. A. (2017). Medium and short term riparian vegetation, Island and channel evolution in response to human pressure in a regulated gravel bed river (Piave River, Italy). Catena, 149, 760–769. https://doi.org/10.1016/j.catena. 2016.04.005
- Poff, N. L., Allan, J. D., Bain, M. B., Karr, J. R., Prestegaard, K. L., Richter, B. D., ... Stromberg, J. C. (1997). The natural flow regime. *Bioscience*, 47(11), 769–784. https://doi.org/10.2307/1313099
- Prior, E. M., Aquilina, C. A., Czuba, J. A., Pingel, T. J., & Hession, W. C. (2021). Estimating floodplain vegetative roughness using drone-based laser scanning and structure from motion photogrammetry. *Remote Sensing*, 13(13), 2616. https://doi.org/10.3390/rs13132616
- Proust, S., Fernandes, J. N., Peltier, Y., Leal, J. B., Riviere, N., & Cardoso, A. H. (2013). Turbulent non-uniform flows in straight compound open-channels. *Journal of Hydraulic Research*, 51(6), 656–667. https://doi.org/10.1080/00221686.2013.818586
- Reclamation. (2012). Hydraulic studies for fish habitat analysis (SRH-2012-15; prepared for San Joaquin River restoration project, mid-Pacific region). US Bureau of Reclamation, Technical Service Center, Denver, CO.
- Rhee, D. S., Woo, H., Kwon, B. A., & Ahn, H. K. (2008). Hydraulic resistance of some selected vegetation in open channel flows. *River Research and Applications*, 24(5), 673–687. https://doi.org/10.1002/rra.1143
- Richardson, D. M., Holmes, P. M., Esler, K. J., Galatowitsch, S. M., Stromberg, J. C., Kirkman, S. P., ... Hobbs, R. J. (2007). Riparian

CHAULAGAIN ET AL. WILEY 1745

- vegetation: Degradation, alien plant invasions, and restoration prospects: Riparian vegetation: Degraded, invaded, transformed. *Diversity and Distributions*, 13(1), 126–139. https://doi.org/10.1111/j.1366-9516.2006.00314.x
- Richardson, J. J., Moskal, L. M., & Kim, S.-H. (2009). Modeling approaches to estimate effective leaf area index from aerial discrete-return LIDAR. Agricultural and Forest Meteorology, 149(6–7), 1152–1160. https://doi.org/10.1016/j.agrformet.2009.02.007
- Saitoh, T. M., Nagai, S., Noda, H. M., Muraoka, H., & Nasahara, K. N. (2012). Examination of the extinction coefficient in the Beer-Lambert law for an accurate estimation of the forest canopy leaf area index. Forest Science and Technology, 8(2), 67–76. https://doi.org/10.1080/21580103.2012.673744
- Sexton, J. O., Bax, T., Siqueira, P., Swenson, J. J., & Hensley, S. (2009). A comparison of lidar, radar, and field measurements of canopy height in pine and hardwood forests of southeastern North America. Forest Ecology and Management, 257(3), 1136–1147. https://doi.org/10.1016/j.foreco.2008.11.022
- Shafroth, P. B., Stromberg, J. C., & Patten, D. T. (2002). Riparian vegetation response to altered disturbance and stress regimes. *Ecological Applications*, 12(1), 107–123. https://doi.org/10.1890/1051-0761(2002)012 [0107:RVRTAD]2.0.CO;2
- Sholtes, J. S., & Doyle, M. W. (2011). Effect of channel restoration on flood wave attenuation. Effect of Channel Restoration on Flood Wave Attenuation, 137, 13–208.
- Solari, L., Van Oorschot, M., Belletti, B., Hendriks, D., Rinaldi, M., & Vargas-Luna, A. (2016). Advances on modelling riparian vegetation-hydromorphology interactions: Modelling vegetation-hydromorphology. River Research and Applications, 32(2), 164–178. https://doi.org/10.1002/rra.2910
- Solberg, S., Næsset, E., Hanssen, K. H., & Christiansen, E. (2006). Mapping defoliation during a severe insect attack on scots pine using airborne laser scanning. *Remote Sensing of Environment*, 102(3-4), 364-376. https://doi.org/10.1016/j.rse.2006.03.001
- Stella, J. C., Rodríguez-González, P. M., Dufour, S., & Bendix, J. (2013). Riparian vegetation research in Mediterranean-climate regions: Common patterns, ecological processes, and considerations for management. *Hydrobiologia*, 719(1), 291–315. https://doi.org/10.1007/s10750-012-1304-9
- Stone, M. C., & Hotchkiss, R. H. (2007). Turbulence descriptions in two cobble-bed river reaches. *Journal of Hydraulic Engineering*, 133(12), 1367–1378. https://doi.org/10.1061/(ASCE)0733-9429(2007)133:12 (1367)
- Stone, M. C., Chen, L., Kyle McKay, S., Goreham, J., Acharya, K., Fischenich, C., & Stone, A. B. (2013). Bending of submerged woody riparian vegetation as a function of hydraulic flow conditions: Bending of submerged woody riparian vegetation. *River Research and Applications*, 29(2), 195–205. https://doi.org/10.1002/rra.1592
- Straatsma, M. W. (2005). Quantitative mapping of hydrodynamic vegetation density of floodplain forests using airborne laser scanning. Photogrammetric Engineering and Remote Sensing, 74(8), 987–998.
- Straatsma, M. W., & Baptist, M. J. (2008). Floodplain roughness parameterization using airborne laser scanning and spectral remote sensing. Remote Sensing of Environment, 112(3), 1062–1080. https://doi.org/ 10.1016/j.rse.2007.07.012
- Sullivan, F. B., Ducey, M. J., Orwig, D. A., Cook, B., & Palace, M. W. (2017). Comparison of lidar- and allometry-derived canopy height models in an eastern deciduous forest. Forest Ecology and Management, 406, 83-94. https://doi.org/10.1016/j.foreco.2017.10.005
- Sweeney, B. W., Bott, T. L., Jackson, J. K., Kaplan, L. A., Newbold, J. D., Standley, L. J., ... Horwitz, R. J. (2004). Riparian deforestation, stream narrowing, and loss of stream ecosystem services. *Proceedings of the National Academy of Sciences*, 101(39), 14132–14137. https://doi.org/ 10.1073/pnas.0405895101

- Thompson, G. T., & Roberson, J. A. (1976). A theory of flow resistance for vegetated channels. *Transactions of ASAE*, 19(2), 288–293. https://doi.org/10.13031/2013.36014
- Tomsett, C., & Leyland, J. (2019). Remote sensing of river corridors: A review of current trends and future directions. River Research and Applications, 35(7), 779–803. https://doi.org/10.1002/rra.3479
- Tseng, Y.-H., Lin, L.-P., & Wang, C.-K. (2016). Mapping CHM and LAI for heterogeneous forests using airborne full-waveform LiDAR data. *Terrestrial, Atmospheric and Oceanic Sciences*, 27(4), 537. https://doi.org/10.3319/TAO.2016.01.29.04(ISRS)
- Uotani, T., Kanda, K., & Michioku, K. (2014). Experimental and numerical study on hydrodynamics of riparian vegetation. *Journal of Hydrodynamics*, 26(5), 796–806. https://doi.org/10.1016/S1001-6058(14)60088-3
- Vermaas, D. A., Uijttewaal, W. S. J., & Hoitink, A. J. F. (2011). Lateral transfer of streamwise momentum caused by a roughness transition across a shallow channel: Lateral roughness change in a shallow channel. Water Resources Research, 47(2), W02530. https://doi.org/10.1029/2010WR010138
- Västilä, K., & Järvelä, J. (2018). Characterizing natural riparian vegetation for modeling of flow and suspended sediment transport. *Journal of Soils and Sediments*, 18(10), 3114–3130. https://doi.org/10.1007/s11368-017-1776-3
- Wang, J., & Zhang, Z. (2019). Evaluating riparian vegetation roughness computation methods integrated within HEC-RAS. *Journal of Hydraulic Engineering*, 145(6), 04019020. https://doi.org/10.1061/(ASCE)HY. 1943-7900.0001597
- Wasser, L., Chasmer, L., Day, R., & Taylor, A. (2015). Quantifying land use effects on forested riparian buffer vegetation structure using LiDAR data. Ecosphere, 6(1), art10. https://doi.org/10.1890/ES14-00204.1
- Wilson, C., Stoesser, T., & Bates, P. D. (2005). Modelling of open channel flow through vegetation. *Computational Fluid Dynamics: Applications in Environmental Hydraulics*, 395–428. https://doi.org/10.1002/0470015195.ch15
- Wohl, E. E. (1998). Uncertainty in flood estimates associated with roughness coefficient. *Journal of Hydraulic Engineering*, 124(2), 219–223. https://doi.org/10.1061/(ASCE)0733-9429(1998)124:2(219)
- Wong, M., & Parker, G. (2006). Reanalysis and correction of bed-load relation of Meyer-Peter and Müller using their own database. *Journal of Hydraulic Engineering*, 132(11), 1159–1168. https://doi.org/10.1061/(asce)0733-9429(2006)132:11(1159)
- Wu, F.-C., Shen, H. W., & Chou, Y.-J. (1999). Variation of roughness coefficients for unsubmerged and submerged vegetation. *Journal of Hydraulic Engineering*, 125(9), 934–942. https://doi.org/10.1061/(ASCE) 0733-9429(1999)125:9(934)
- Wunder, S., Lehmann, B., & Nestmann, F. (2011). Determination of the drag coefficients of emergent and just submerged willows. *International Journal of River Basin Management*, 9(3–4), 231–236. https://doi.org/10.1080/15715124.2011.637499

## SUPPORTING INFORMATION

Additional supporting information can be found online in the Supporting Information section at the end of this article.

How to cite this article: Chaulagain, S., Stone, M. C., Dombroski, D., Gillihan, T., Chen, L., & Zhang, S. (2022). An investigation into remote sensing techniques and field observations to model hydraulic roughness from riparian vegetation. *River Research and Applications*, 38(10), 1730–1745. https://doi.org/10.1002/rra.4053